SCIENTIFIC REPORTS

OPEN

Correspondence and requests for materials should be addressed to A.H.L. (liuah@qibebt.ac.cn); C.C.L. (chm_licc@ujn.edu.cn) or V.A.P. (petreva@auburn.edu)

Bio-mimetic Nanostructure Self-assembled from Au@Ag Heterogeneous Nanorods and Phage Fusion Proteins for Targeted Tumor Optical Detection and Photothermal Therapy

Fei Wang[1], Pei Liu[1], Lin Sun[2], Cuncheng Li[2], Valery A. Petrenko[3] & Aihua Liu[1]

[1]Laboratory for Biosensing, Qingdao Institute of Bioenergy & Bioprocess Technology, and Key Laboratory of Biofuels, Chinese Academy of Sciences, 189 Songling Road, Qingdao 266101, China, and University of Chinese Academy of Sciences, 19A Yuquan Road, Beijing 100049, China, [2]Key Laboratory of Chemical Sensing & Analysis in Universities of Shandong, School of Chemistry and Chemical Engineering, University of Jinan, Jinan 250022, China, [3]Department of Pathobiology, Auburn University, 269 Greene Hall, Auburn, Alabama 36849-5519, United States.

Nanomaterials with near-infrared (NIR) absorption have been widely studied in cancer detection and photothermal therapy (PTT), while it remains a great challenge in targeting tumor efficiently with minimal side effects. Herein we report a novel multifunctional phage-mimetic nanostructure, which was prepared by layer-by-layer self-assembly of Au@Ag heterogenous nanorods (NRs) with rhodamine 6G, and specific pVIII fusion proteins. Au@Ag NRs, first being applied for PTT, exhibited excellent stability, cost-effectivity, biocompatibility and tunable NIR absorption. The fusion proteins were isolated from phage DDAGNRQP specifically selected from f8/8 landscape phage library against colorectal cancer cells in a high-throughput way. Considering the definite charge distribution and low molecular weight, phage fusion proteins were assembled on the negatively charged NR core by electrostatic interactions, exposing the N-terminus fused with DDAGNRQP peptide on the surface. The fluorescent images showed that assembled phage fusion proteins can direct the nanostructure into cancer cells. The nanostructure was more efficient than gold nanorods and silver nanotriangle-based photothermal agents and was capable of specifically ablating SW620 cells after 10 min illumination with an 808 nm laser in the light intensity of 4 W/cm². The prepared nanostructure would become an ideal reagent for simutaneously targeted optical imaging and PTT of tumor.

P hotothermal therapy (PTT) is one of the most promising methods in cancer treatment, which can induce irreversible damage to cancer cells in a mild way by generating hyperthermia and avoid side effects to healthy tissues[1]. To date, multifunctional nanomaterials with high optical absorption in the near-infrared (NIR) region have been widely explored for PTT, including gold nanoparticles[2–4], bimetallic nanostructures[5–7], carbon nanomaterials[8–10] and palladium nanosheets[11,12]. Among them, noble metal nanomaterials draw great interest because of their higher photothermal efficiency, which is generated by their unique attribute of surface plasmon resonance (SPR)[13]. For successful application of noble metal nanomaterials in PTT, they have to be targeted to cancer cells to force their specific photothermal ablation[14–16]. To increase their specific affinity toward target cancer cells, nanoparticles have been conjugated with antibodies, short peptides, aptamers, folates and other targeted molecules through covalent binding or physical absorption[17]. However, efficiency of covalent binding can vary depending on functional moieties and coupling agents in the complex, as well as multistep chemical reactions. Furthermore, specific biological molecules are apt to change the conformation and lose their activities during this post-modification[18]. Physical absorption, operating through the electrostatic interaction, van der Waals forces, hydrogen bonds or hydrophobic interactions, allows normally conserving conformation of the
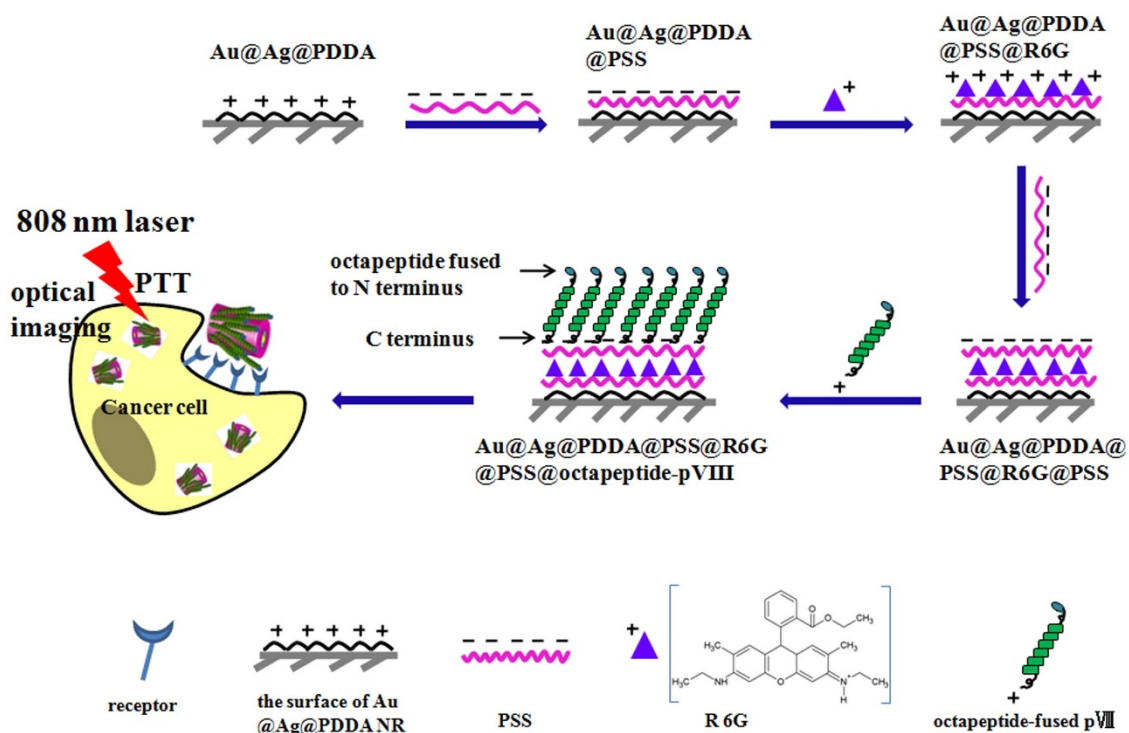
Figure 1 | **This scheme depicts the LbL assembly of PMHNR.** The Au@Ag heterogenous NR with the polycationic PDDA as the stabilizer was used as the core to construct the negatively charged Au@Ag@PSS@R6G@PSS NR by depositing polyanionic PSS and positively charged R6G molecules on the surface by LbL assembly. The pVIII fusion proteins were isolated from the SW620 cell-specific phage, which was selected from the f8/8 landscape phage library. Through the positively charged C terminus, the pVIII fusion proteins should readily assemble onto the surface of Au@Ag@PDDA@PSS@R6G@PSS NRs to generate PMHNRs, which retains their specific octapeptide at N terminus outwardly. The resultant biomimetic nanostructure can be used for specific optical imaging and PTT of cancer cells.

attached ligand, although its application for conjugation of target molecules can be also limited by heterogeneous charge distribution over their surface and randomly spatial orientation of molecular functional domains in their conjugated forms[18,19]. Moreover, high molecular weight proteins may change their size and shape when absorbed to nanomaterials[18]. Therefore, there is an urgent need in discovering of specific ligands with definite charge distribution, low molecular weight and high specificity for targeted delivery and PTT application of noble metal nanomaterials.

The phage display technique provides a powerful method to explore specific ligands as substitute of antibodies to certain targets[20–22]. The common vector in phage display, Fd phage, belongs to F-specific filamentous phages, which infect Gram-negative bacteria carrying the F-factor without killing the host[23]. The 6,400-nucleotide ssDNA of fd phage is encapsulated by protein coats including 2,700 copies of pVIII major coat protein and about five copies each of four minor coat proteins (Fig. S1A)[24]. The wild-type pVIII protein is composed of 50 amino acids that form an extended α helix including the hydrophobic transmembrane domain, the negatively charged N terminus, and the positively charged C terminus[24]. The multiple copies of pVIII coat protein are assembled with the N terminus exposing on the outer surface of the capsid and the C terminus oriented inside the capsid interacting with phosphates of ssDNA[24].

Landscape phage library containing about 2×10^9 individual clones bearing different exogenous peptides, has been developed by one of our coauthors by fusing random octapeptides to the N terminus of all 4,000 copies of pVIII major coat protein in fd-tet phage (Fig. S1B)[25]. The diversity of the landscape library and multivalent property of individual landscape phage make it an ideal resource to select specific ligands with high-affinity in a high-throughput fashion[26]. The pVIII major coat proteins with N terminal cancer cell-specific octapeptides have been successfully employed as target

ligands for chemotherapy in physically assembled compositions with liposomes, micelles or siRNA for targeted delivery of drugs, DNA or siRNA[27–29], or chemically modified on the surface of inorganic nanoclusters for targeted gene delivery[30]. However, there are no reports on using of specific pVIII fusion proteins as targeted ligands to assemble with noble metal nanoparticles for the PTT application to tumor.

Here, we report novel multifunctional phage protein-modified Au@Ag heterogeneous nanorods (PMHNRs) for targeted optical detection and PTT towards colorectal carcinoma cells SW620. PMHNRs were prepared by self-assembling Au@Ag heterogeneous NRs with polyanionic poly(styrenesulfonate) (PSS), rhodamine 6G (R6G) and specific pVIII fusion proteins (Fig. 1). The designed PMHNRs have several characteristic superior features in comparison with other materials used in PTT. First, the stable Au@Ag heterogeneous NRs can be synthesized by a simple and controllable one-pot method with high-yield[31]. These NRs have two strong absorption peaks and the longitudinal absorption peak can be facilely turned as expected to the NIR region, overlapping with the tissue window for *in vivo* PTT. Compared with the prevalent gold nanorods (GNRs) used as PTT agent, Au@Ag heterogenous NRs are less expensive because silver is their main composition. Second, due to the presence of strong positively charged poly(diallyldimethylammonium) chloride (PDDA) on the surface as stabilizer, the Au@Ag heterogeneous NRs have excellent stability, that is quite important for their applications based on the plasmonic property[31]. Thus, Au@Ag heterogeneous NR would provide an ideal core for layer-by-layer (LbL) assembly. Moreover, compared with the cytotoxic cetyltrimethylammonium bromide (CTAB) molecules coated on the GNRs, the polymer PDDA has not been reported for any cytotoxicity, which provides Au@Ag heterogeneous NRs excellent potential in PTT applications for cancer cells. Third, cancer cell-specific phage can

be selected from the f8/8 landscape phage library in a high-through-put way and phage fusion proteins pVIII can be easily obtained by disassembling the amplified phage (Fig. S1; Fig. S2). Finally, the exact charge distribution of pVIII coat proteins makes them suitable for being physically reassembled *in vitro* with the negatively charged core through electrostatic interaction, mimicking the phage self-assembly between ssDNA and coat proteins. As shown in Fig. 1, SW620 cell-specific pVIII-fused peptides were assembled with Au@Ag heterogeneous NRs through electrostatic interactions mediated by multilayers of polyelectrolytes and fluorescent probes, resulting in a stable and biocompatible complex. Due to the unique dipole properties of the pVIII protein, the negatively charged N terminus of the SW620 cell-specific octapeptide is exposed outward of the PMHNRs, therefore, the specificity of the targeted PTT is highly facilitated. Thus, the PMHNRs first described in this paper can find potential applications in simultaneous specific optical imaging and efficient ablation of cancer cells.

Results

Selection of SW620 Cell Specific Phage. We discovered the SW620 cell specific ligand from the f8/8 landscape phage library for the first time (Fig. S2). SW620 cell-binding phages were selected using a stringent library depletion protocol. In order to minimize the nonspecific binding and increase the efficiency and specificity of selection, the original library was sequentially depleted against culture plates, serum and control cells (normal fetal kidneys cell line HEK293T and hepatocellular carcinoma cell line HepG2) before incubation with the target SW620 cells. Moreover, all washing steps were rigorous in 3 rounds of selection to eliminate unbound and weakly binding phages. For each round of selection against SW620 cells, phages binding on the surface and internalizing into cells were collected from the elution buffer or the cell lysate respectively. Phages from the eluate and lysate fraction were amplified separately and used as the input in the next round of selection. The phage recovery rate of each round that calculated as the ratio of output to input phages was increased progressively in the selection procedure, which indicated that phages binding with SW620 cells were successfully enriched from f8/8 landscape phage library (Fig. S3). After 3 rounds of selection, 5 phage clones separated from the surface and interior of SW620 cells were randomly picked up for PCR amplification and sequencing. The sequences and frequencies of SW620 cell-binding octapeptides were shown in Table S1. Three unique octapeptides were identified from ten selected phage clones. The phage DDAGNRQP (called C1 phage)

and DFAPVDGQ (called C2 phage) were isolated from both the surface and interior fraction with higher frequency than another one.

The specificity and affinity of phages binding to SW620 cells were identified by phage capture assay. Among three isolated phages, the recovery frequency of C1 phage and C2 phage were higher than that of DHTASWST phage, so these phages were chosen for specificity and affinity assay (Table S1). As shown in Fig. 2, there was no C1 phage binding with HepG2 and HEK293T cells according to the phage recovery rate. Actually, the output phages were counted based on the number of corresponding colonies, so when the number of phage particles in the eluate was less than 40 TU (titer unit), there were no colonies on the plate and the phage recovery rate was considered as zeto. Therefore, the calculated level of C1 phage binding with SW620 cells was much higher than with control groups, which demonstrated high specificity of phages towards the target SW620 cells (Fig. 2). Compared with C1 phage, C2 phage bound not only SW620 cells but also HepG2 cells (Fig. 2). Moreover, the recovery rate of C2 phage from the target group was almost 3-fold lower than that of C1 phage, indicating that C1 phage had better affinity to SW620 cells (Fig. 2). Considering the high specificity and affinity, DDAGNRQP was chosen as the specific ligand to SW620 cells.

Self-assembly and Characterization of PMHNRs. The variants of phage fd-tet that we discovered in this work, contain about 4,000 copies of pVIII coat protein that constitute about 90% of phage mass. They can be extracted from the phage by saturated phenol, detergents, or organic solvents (Fig. S2)[32,33]. The ratio of the absorbance at 280 nm (A280) to the absorbance at 260 nm (A260) (A280/A260) was calculated to be 1.674, indicating that the phage DNA was eliminated[34]. The speculated molecular weight of DDAGNRQP-fused pVIII protein is approximately 5.79 kDa with 55 amino acids. The tricine-SDS-PAGE assay showed that the DDAGNRQP-fused pVIII proteins were isolated as the dimers with the molecular weight of about 12 kDa (Fig. S4).

The Au@Ag heterogenous NRs were synthesized by a PDDA-mediated polyol process[31]. The aspect ratio of the synthesized NRs was about 3.14 with the average length of 220 nm and width of 70 nm from the transmission electron microscopy (TEM) image (Fig. 3A). Using the PDDA as the shape-controller and stabilizer, the NRs showed excellent stability and monodispersity. As shown in Fig. 3B, the Au@Ag heterogenous NRs had two strong optical absorption peaks locating at 401 and 803 nm, which were attributed to the transverse and longitudinal electron oscillations, respectively. It is known that the light penetration window in the biological tissue is in the NIR region ranging from 650 to 900 nm, where the hemoglobin and water has minimal light absorption. Therefore, the Au@Ag heterogenous NR with 803 nm absorption is an ideal candidate for tumor PTT.

In order to optically detect and photothermal ablate SW620 cells specifically, multifunctional PMHNRs were constructed by LbL assembly of Au@Ag heterogenous NRs with dye molecules and DDAGNRQP-fused pVIII proteins. As shown in Fig. 4, the zeta potential of the synthesized Au@Ag@PDDA NRs is 41.1 mV with the polycationic PDDA on the surface. Then, these NRs were treated with polyanionic PSS to generate the negatively charged conjugate Au@Ag@PDDA@PSS NRs (Fig. 4). Following that, the positively charged R6G dye molecules were deposited on the anionic PSS-ter-minating surface to generate Au@Ag@PDDA@PSS@R6G NRs, for which the zeta potential reversed from −9.6 mV to 33.0 mV (Fig. 4). Finally, DDAGNRQP-fused pVIII proteins were assembled on the surface of the conjugate Au@Ag@PDDA@PSS@R6G@PSS NRs to obtain PMHNRs, and the final zeta potential changed from −24.2 mV to −0.88 mV (Fig. 4). The reversal of zeta potentials revealed that the C terminus of pVIII fusion protein was conjugated with the negatively charged Au@Ag@PDDA@PSS@R6G@PSS NRs and the weakly negatively charged N terminus with two acidic amino
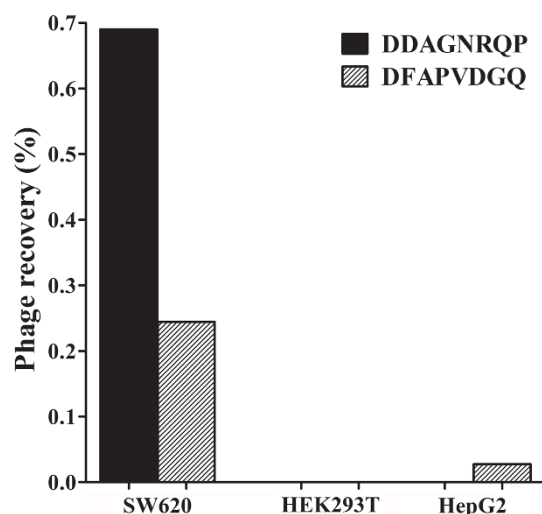
**Figure 2 | Specificity and affinity testing of selected phage clones displaying DDAGNRQP and DFAPVDGQ respectively.**
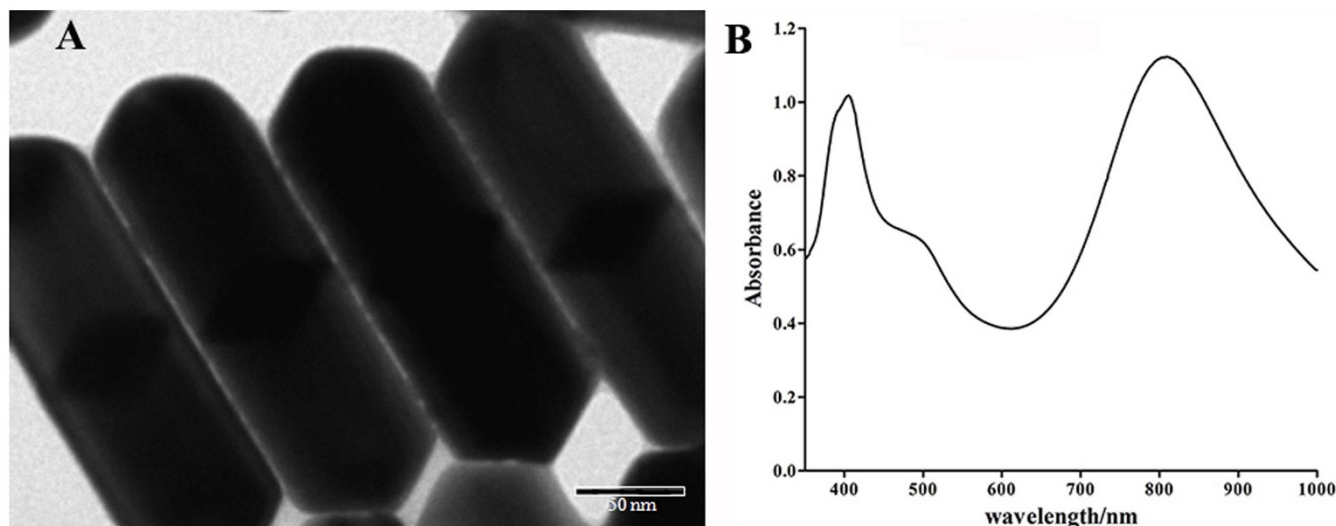
Figure 3 | (A) TEM image and (B) UV-Vis-NIR absorption spectra of the synthesized Au@Ag heterogenous NRs.

acids (aspartic acid) and one basic amino acid (arginine) was exposed on the surface (Fig. 1).

The morphology of NRs in the LbL assembly process was characterized by TEM. As shown in Fig. 5, the outer layer (the grey portion around the NR) of the NRs became thicker as the LbL assembly processed. Compared with Au@Ag@PDDA NRs (Fig. 5A), the increase in outer layer thickness for Au@Ag@PDDA@PSS NRs (Fig. 5B) was not quite obvious, because the persistence length of PSS was only about 1 nm[35,36]. However, the outer layer thickness of PMHNRs was about 4 nm, which is thicker than that of Au@Ag@ PDDA NRs due to additional 2 layers of PSS and 1 layer of pVIII fusion proteins deposition on the surface (Fig. 5C). The UV-Vis-NIR absorption spectra showed that the longitudinal absorption peak gradually red-shifted from 803 to 810 nm due to the surface layers added, as a result of slight changes in the aspect ratio (Fig. 6; Fig. S5). Ultimately, the above results suggested the successful construction of PMHNRs by controllable LbL assembly.
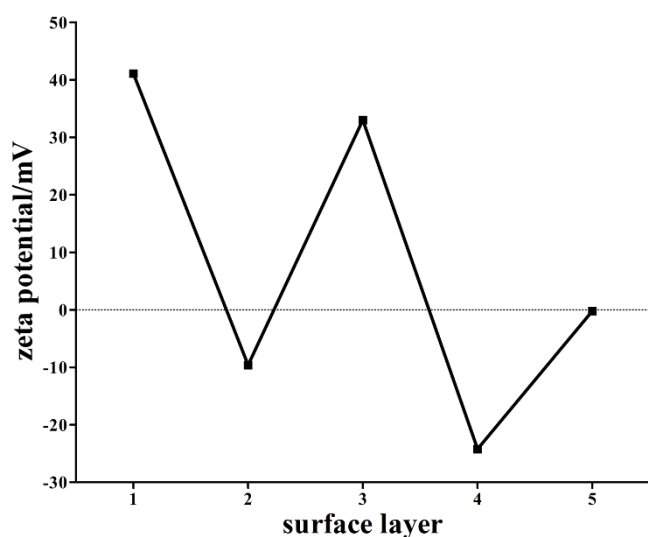

Figure 4 | The reversal of zeta potential of bio-nanocomposite as surface layer of Au@Ag heterogenous NRs added during the assembling process. The surface layer number of 1 to 5 corresponded to Au@Ag@PDDA NRs, Au@Ag@PDDA@PSS NRs, Au@Ag@PDDA@PSS@R6G NRs, Au@Ag@ PDDA@PSS@R6G@PSS NRs and PMHNRs, separately.

PMHNRs-Based Selective Optical Detection and Photothermal Therapy of Cancer Cells. To check cytotoxicity of Au@Ag heterogeneous NRs and PMHNRs, they have been incubated with control and target cells, and cell viability was evaluated by 3-(4,5-dimethylthiazol-2-yl)-2,5-diphenyltetrazolium bromide (MTT) assay. As shown in Fig. S6, cell viability was still higher than 80% when the concentrations of both nanoparticles reached 200 μg/ml, indicating that the PMHNRs can be used for tumor PTT both *in vitro* and *in vivo*. The selective binding of PMHNRs to SW620 cells and their intracellular distribution was investigated by confocal fluorescence microscopy of different cells and by ultrathin TEM. The fluorescence was quenched obviously when R6G molecules were encapsulated within PMHNRs, but the signal was observed after intermittent irradiation for 10 min in the power of 100 mW, which was attributed to the release of R6G molecules (Fig. S7). When the irradiation time reached 60 min, the fluorescence intensity was high enough to be used for imaging of cancer cells (Fig. S7). Following incubation with PMHNRs for 4 h and intermittent irradiation with an 808 nm laser for 60 min, target group showed strong red color around SW620 cells corresponding to R6G molecules, while control cells had no fluorescence signals (Fig. 7). PMHNRs in vesicles were observed in the ultrathin TEM images of SW620 cells, which further demonstrated that PMHNRs with monodispersity were endocytosed through the interaction of specific ligands and receptors into cell cytoplasm (Fig. S8). These data allowed us to conclude that the isolated DDAGNRQP-fused pVIII coat proteins retained their targeted recognition capability after being re-assembled with Au@Ag heterogeneous NRs.

To investigate the role of light power in PTT of PMHNRs towards SW620 cells, we applied three kinds of light intensity at 808 nm to SW620 cells after they were treated with PMHNRs. When the light intensity was 0.8 W/cm² or 2 W/cm², cell viability can still keep above 80% even if the constant illumination time reached 30 min (Fig. S9). When the light intensity was as high as 4 W/cm², most cells were dead after constant 10 min illumination and the cell viability was only 30% after constant 30 min illumination (Fig. S9). The SW620 cell viability after treatment with different light intensity showed that the light intensity of 4 W/cm² was sufficiently powerful for photothermal applications of Au@Ag heterogeneous NRs.

All cells were exposed to 808 nm laser for different time in the light intensity of 4 W/cm² after incubation with PMHNRs for 6 h. Control cells had the viability above 80%, and even if the irradiation time was as long as 30 min, cells were slightly influenced (Fig. 8). HepG2 cells died faster than HEK293T cells, probably because cancer cells are more sensitive to high temperature than normal cells or
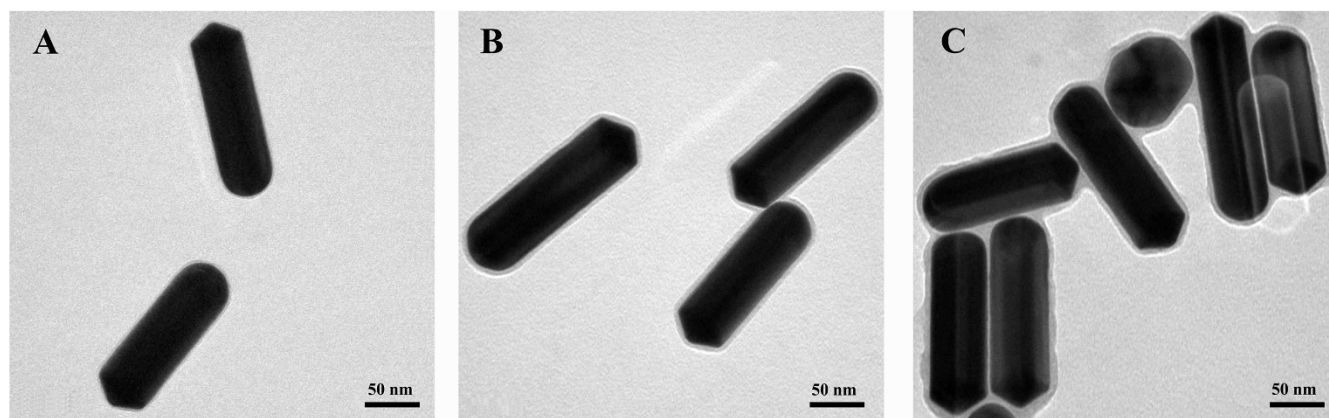
Figure 5 | TEM images of Au@Ag@PDDA NRs (A), Au@Ag@PDDA@PSS NRs (B) and PMHNRs (C). The surrounding grayish layer was the outer surface of the Au@Ag heterogenous NR. The samples were stained with 1% uranyl acetate before measurement.

PMHNRs were internalized into HepG2 cells at slightly higher level that into HEK293T cells. As shown in Fig. 8, a large number of SW620 cells died after 10 min constant illumination. It was supposed that sufficient amount of PMHNRs were endocytosed to generate enough heat to ablate SW620 cells under constant light irradiation. Our results indicated that PMHNRs assembled with DDAGNRQP-fused pVIII coat proteins can specifically interact with the target and

effectively generate hyperthermia to ablate SW620 cells at a lower irradiation power.

Discussion

Noble metal nanomaterials received great attention in tumor PTT because of their intrinsic property of SPR, which can rapidly convert light to heat. Currently, nanomaterials were located or delivered to
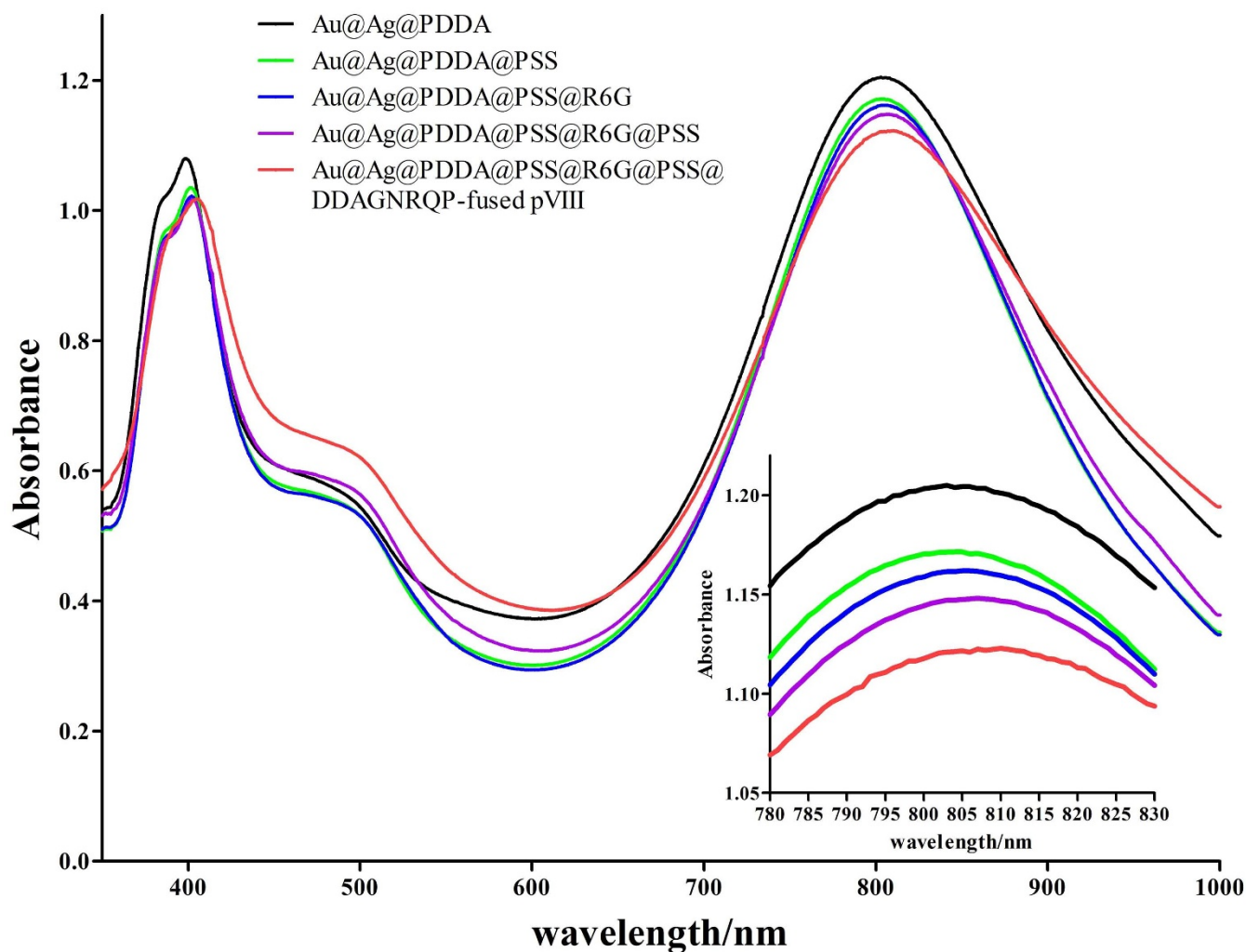
Figure 6 | UV-Vis-NIR absorption spectra of Au@Ag heterogenou NRs upon LbL surface assembly. Inset, the enlarged portions of the spectra ranging from 780 to 830 nm.
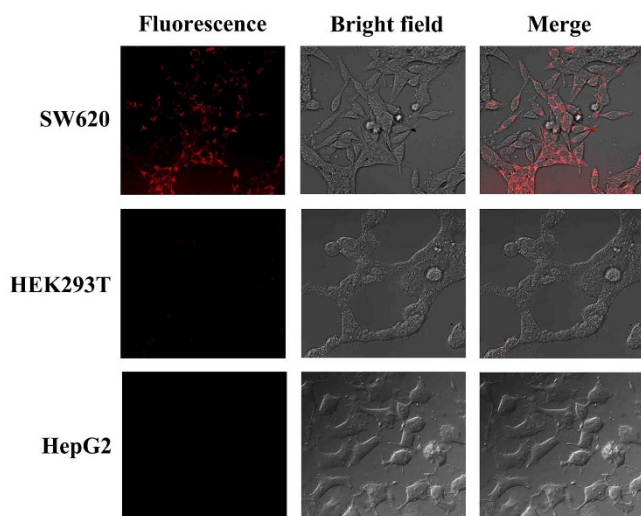
Figure 7 | Confocal fluorescence images of SW620, HEK293T and HepG2 cells after incubation with PMHNRs for 4 h.

Figure 8 | The cell viability of HepG2, HEK293T and SW620 cells varying with irradiation time. The selective PTT was tested with an 808 nm laser (4 W/cm²) after the cells incubation with 50 μg/ml PMHNRs for 6 h. (*$p < 0.05$, mean ± standard deviation, n = 3).

the target by exploiting the enhanced permeability and retention effect of tumor vessels. However, nanomaterials in the passive targeting are accessible to normal tissues and their utilization was limited by the particular size. Therefore, it is of great importance to exploring novel specific ligands for active targeting of tumor to minimize the side effects of nanomaterials. Here, we constructed the multifunctional nanostructure PMHNRs for specifically optical detection and photothermal ablation of cancer cells.

Specific proteins, peptides, antibodies and aptamers are commonly attached on nanomaterials for active targeting to tumor. But the high cost, high molecular weight and instability hindered their effective application as the target molecules of nanomaterials. Phage display provides an excellent approach to discover the specific ligands against various targets without knowledge about their molecular properties. The filamentous phages displaying foreign peptides on the surface have been constructed and used in immunoassay, drug delivery and biosensing[37–41]. Several kinds of colorectal cancer-targeting peptides have been selected from the pIII display libraries[42]. However, the specific pIII fusion protein has just five copies at the tip of the phage, which can't be obtained in large quantities. Thus, the f8/8 landscape phage library based on type VIII display system was screened against SW620 cells, and C1 phage displayed the peptide DDAGNRQP with high specificity and affinity was selected as the SW620 cell specific ligand (Fig. 2). The peptide DDAGNRQP was different from the reported peptides, which may be attributed to the variety of phage display libraries and the diversity of cell lines[42]. The DDAGNRQP-fused pVIII coat proteins were purified based on the different solubility of DNA and protein in the aqueous solution. The isolated pVIII fusion protein was a dimer with the molecular weight of about 12 kDa (Fig. S4). It has been demonstrated that the pVIII coat protein is highly hydrophobic and insoluble in water, so oligomeric or polymeric state of pVIII proteins are commonly observed in the liposomes or micelles[43]. Compared with commercial targeting molecules, phage pVIII fusion protein exhibited definite charge distribution, low molecular weight, high valence and stability.

Viruses with well-defined properties and abundant coat proteins have been widely used to construct multifunctional virus-like nanoparticles using self-assembly technique[44]. As the phage DNA is negatively charged due to the presence of multiple phosphate groups, the positively charged lysine-rich C terminus of pVIII coat proteins interacts with the DNA core while the acid domain of N terminus fused with guest peptide is accommodated on the surface[45]. Inspired by nature, we attempted to assemble the pVIII-fused DDAGNRQP
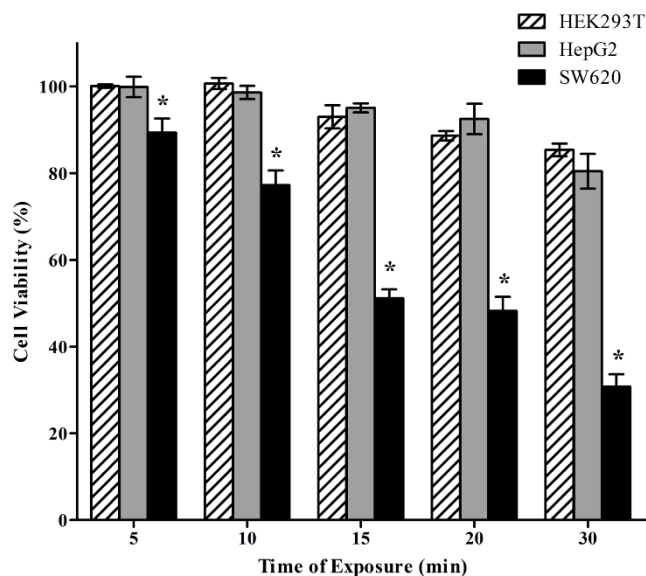
with the negatively charged PTT agent to construct multifunctional phage-mimetic nanostructure. Au@Ag heterogenous NRs with the absorption peak of 803 nm were synthesized as tumor PTT agent (Fig. 3), because the hemoglobin and water has minimal light absorption in the NIR region ranging from 650 to 900 nm[46]. The surface of Au@Ag heterogenous NRs is positively charged due to the presence of polycationic PDDA as a stabilizer on the surface. These NRs were treated with polyanionic PSS to form the negatively charged conjugate Au@Ag@PDDA@PSS NRs (Fig. 1). In order to trace the location of Au@Ag heterogenous NRs, the positively charged R6G dye molecules were trapped in multilayers of the anionic PSS to generate the conjugate Au@Ag@PDDA@PSS@R6G@PSS NRs (Fig. 1). Finally, pVIII-fused DDAGNRQP proteins were assembled through the positively charged C terminus onto the conjugate Au@Ag@PDDA@PSS@R6G@PSS NRs to generate PMHNRs, which retained their SW620 cell-specific octapeptide DDAGNRQP at N terminus outwardly (Fig. 1). The reversal of zeta potentials and the red-shift of the longitudinal absorption peak confirmed that the resultant PMHNRs encapsulating dye molecules and being covered with specific pVIII fusion proteins were successfully constructed for targeted fluorescent detection and PTT of SW620 cells (Fig. 4; Fig. 5; Fig. 6).

So far, GNR has been widely used for tumor PTT, which was synthesized using CTAB as the template and stabilizer[2]. However, it is well-known that CTAB is cytotoxic to cells, therefore, CTAB-coated GNRs could not be used in vivo[47]. The synthesized Au@Ag heterogeneous NRs were coated with PDDA, a cationic polyelectrolyte with unknown cytotoxicity. Although some reports argued that silver nanoparticles may be toxic, the toxic effects have been proved to be dose-dependent and depended on their size, shape, surface modification and charge[48–50]. Moreover, silver nanoparticles have been widely used in antimicrobial therapy and wound dressings in clinic[51]. Importantly, we found that both the Au@Ag heterogeneous NRs and their biocomposites have little toxicity on the incubated cells (Fig. S6), suggesting their perfect biocompatibility.

The confocal fluorescence microscopy (Fig. 7) and ultrathin TEM images (Fig. S8) confirmed that the assembled pVIII proteins retained their targeting capability and directed the PMHNRs being specifically uptaken by SW620 cells. As expected for the fluorescent signal of dye molecules on the metal surface, the enhancement or quenching was distance-dependent[52]. It has been reported that dye

molecules can be released from polyelectrolyte layers on the surface of metal nanoparticles under controllable light illumination[53]. The fluorescence spectra suggested that increasing R6G molecules were induced to release from the surface of PMHNRs when the irradiation time was gradually prolonged to generate enough plasmonic heating (Fig. S7). It has been proved that nanoparticles with positive charge exhibit high cellular uptake, while those with negative charge or close to neutral charge are unable to enter cells easily through electrostatic interaction with cell surface[54]. Thus, it was confirmed that PMHNRs with zeta potential of −0.88 mV were taken by SW620 cells at high level mainly through targeted interaction.

It has been reported that cancer cells incubated with GNRs were effectively ablated by irradiation for at least 4 min with light intensity above 10 W/cm[2][22,55]. Silver nanotriangles with NIR absorption were also tested as photothermal agents. It was found that they need 10 min irradiation with light intensity above 10 W/cm^{2} to generate enough hyperthermia to ablate cancer cells[56]. According to the results of different cell viability, the light power 4 W/cm^{2} is sufficient for Au@Ag heterogeneous NRs to generate hyperthermia (Fig. 8). Therefore, Au@Ag heterogeneous NRs studied in this work were more effective in photothermal applications, probably because the plasmon intensity of sliver nanorods is stronger than that of GNRs and they are able to transfer the energy to heat more effectively[57].

In summary, in order to improve the tumor targeted efficiency of nanoparticles and realize the simultaneous fluorescence imaging detection and PTT of cancer cells, we developed novel multifunctional PMHNRs by assembling DDAGNRQP-fused pVIII proteins with Au@Ag heterogeneous NRs mediated by polyelectrolytes and dye molecules by controllable LbL self-assembly. The Au@Ag heterogenous NRs, as the core of PMHNRs, were proved to have high stability, monodispersity and good biocompatibility. The DDAGNRQP-fused pVIII proteins were isolated in milligram quantity from the SW620 cell-specific phage, which was initially selected from the f8/8 landscape phage library in a high-throughput way. Because of the unique dipole properties of the pVIII fusion protein, its positively charged C terminus was assembled on the negatively charged surface of Au@Ag@PDDA@PSS@R6G@PSS NR, exposing its N terminus fused with the specific DDAGNRQP peptide on the NR surface. The assembled PMHNRs carrying the SW620 cell-specific pVIII fusion protein intensively absorbed light at the 810 nm and specifically ablated the target SW620 cells under constant 10 min illumination with an 808 nm laser at the light power 4 W/cm^{2}. Because of their good biocompatibility and strong NIR absorption, the PMHNR biomimetic nanostructure may be used as an ideal reagent for targeted PTT of tumor.

Methods

Materials and Reagents. Human colorectal carcinoma cells SW620 were kindly gifted by Dr. Yong Cheng in the First Affiliated Hospital of Chongqing Medical University (Chongqing, China). Fetal kidneys cells HEK293T were generously provided by Dr. Songshan Jiang in Sun Yan-Sen University (Guangzhou, China). Human hepatocellular carcinoma cells HepG2 were kindly gifted by Dr. Hongshan Wei in Beijing Ditan Hospital Medical University (Beijing, China). Dulbecco's modified Eagle's medium (DMEM) medium, fetal bovine serum (FBS), bovine serium albumin (BSA) and MTT were purchased from Salarbio (Beijing, China). Dimethyl sulfoxide (DMSO) was purchased from Amresco (Solon, OH, U.S.). Chloroauric acid (HAuCl$_4$, 99%), silver nitrate (AgNO$_3$, ≥99.8%) and PDDA (MW = 100,000–200,000, 20 wt % in water) were purchased from Sigma-Aldrich. PSS (MW = 70,000) was purchased from J&K Scientific (Beijing, China). R6G dye was purchased from Aladdin (Shanghai, China). Sodium deoxycholate, Tween 20 and tris(hydroxymethyl)-aminomethane (Tris) were purchased from Sinopharm Chemical Reagent Co., Ltd. (Shanghai, China) and used without further purification. The 30 cm^2 polystyrene flasks and 96-well cell culture plates were purchased from Corning (New York, U.S.).

The F8/8 Landscape Phage Library. The f8/8 landscape phage library was constructed by one of our co-workers based on type 8 display system[25]. In this system, the synthesized random oligonucleotide encoding octapeptide replaced the nucleic acids of *gVIII* encoding N terminal Glu-Gly-Glu (E2-G3-E4) peptide, resulting in up to 4,000 copies of random octapeptide displayed on the surface of individual phage[25,58]. The f8/8 landscape phage library contains about 2 × 10^9

different clones. All procedures for phages propagation, purification, titration, isolation of phage DNA and PCR identification have been described previously[22].

Specificity Testing of SW620 Cell-Binding Phage Clones. The specificity of SW620 cell-binding phages were determined by phage capture assay in a 96-well cell culture plate[34]. Briefly, SW620, HEK293T and HepG2 cells were cultivated to 90% confluence in individual microwell at 37°C overnight. All cells were washed twice, and then incubated with serum-free DMEM medium for 1 h at 37°C. SW620 cell-binding phages (1 × 10^6 cfu) in 50 μl blocking buffer were separately added to the each well with different cells and incubated for 1 h at room temperature (RT). Cells were washed 8 times with 100 μl of washing buffer for 5 min to remove unbound phages. Elution buffer was added to each microwell and incubated for 10 min on ice to collect phages binding to cells. The eluate from every well was transferred to a centrifuge tube and neutralized as above. All cells were washed with serum-free DMEM medium and treated with lysis buffer to recover cell-internalizing phages. The concentration of phage particles from every fraction was measured by titrating, and phage recovery was calculated as the ratio of input to output phages.

Synthesis of Au@Ag Heterogeneous NRs. Au@Ag heterogenous NRs were synthesized by the one-pot method which we have reported previously[31]. Briefly, 0.05 ml of 0.5 M HAuCl$_4$ aqueous solution, 1.2 ml of 1.25 mmol PDDA, and 0.5 ml of 0.5 M AgNO$_3$ aqueous solution were added to 49 ml of ethylene glycol (EG) solution in a brown glass vial. The mixture was vigorously stirred about 30 s at RT under ambient conditions, and then incubated at 200°C for 72 h in an oil bath. After centrifugation at 14,500 rpm, the supernatant became clear and the precipitate was washed repeatedly with distilled water and ultrasound to remove any residual EG or PDDA. The physical and optical properties of final brown products were characterized for further study.

Self-assembly of PMHNRs. In order to obtain multifunctional SW620 cell-targeted PMHNRs, the Au@Ag heterogeneous NRs were encapsulated with polyelectrolyte, charged dye molecules and pVIII fusion proteins by LbL self-assembly. Shortly, the synthesized Au@Ag heterogeneous NRs were capped with positively charged PDDA. NRs were centrifuged at 8,000 rpm for 20 min twice to remove the excess PDDA and resuspended in water. The positively charged NRs were added to the 10 mg/ml PSS solution (containing 50 mM NaCl) and vigorously stirred over 2 h, converting the positively charged surface to negatively charged[59]. The solution was centrifuged at 8,000 rpm for 20 min to remove the excess PSS, and the pellet was resuspended in NaCl buffer (pH 7.0). The negatively charged surface of PSS-coating NRs was reconverted to positively charged surface by mixing the samples with R6G molecules using the same strategy[60]. After centrifugation and dispersion, the positively charged Au@Ag@PDDA@PSS@R6G NRs were added to PSS solution and operated in the same way, and then negative charged Au@Ag@PDDA@PSS@R6G@PSS NRs were obtained. The SW620 cell-specific pVIII fusion proteins in 50 mM sodium deoxycholate buffer, prepared as described above, were added to the negatively charged Au@Ag@PDDA@PSS@R6G@PSS NRs solution under the vigorous stirring and dialysized against 2 L of deioinized water. The finally prepared PMHNRs were collected by centrifugation and resuspended in PBS (pH 7.0) buffer for the subsequent experiments.

Plasmonic Photothermal Release of R6G from PMHNRs. The synthesized PMHNRs were dispersed in distilled water in microcentrifuge tubes. The individual sample was exposed to an 808 nm laser with a power of 100 mW in 5 min interval for different time. Then the fluorescence spectra of the samples were measured.

Specificity Assay of PMHNRs. The specific detection of cancer cell using PMHNRs was performed by the confocal fluorescence imaging and ultrathin TEM imaging. Cells were cultured on glass bottom dish for 24 h at 37°C. Prepared PMHNRs in serum-free DMEM medium were incubated with cells for 4 h at 37°C. The medium was removed and cells were washed several times with PBS buffer. Then, one part of the sample was intermittently irradiated with 808 nm laser in 5 min interval for 60 min to release the R6G dye molecules which were entrapped in polyelectrolytes[53]. Subsequently, PBS buffer was removed and cells were cultured in DMEM medium with 10% FBS at 37°C. The confocal fluorescent images of individual examples were recorded. Then, the other part of cells were fixed by 2.5% glutaraldehyde and washed with PBS buffer for three times. Fixed cells were stained by OsO$_4$ for 1 h and dehydrated with graded acetone. Cells were further embedded in the pure resin and cut to the ultrathin section for TEM imaging.

Photothermal Therapy. For photothermal therapy of cancer cells *in vitro*, they were irradiated using a diode laser of 808 nm wavelength with controllable power density. Cells were cultivated to 80% confluence in 96-well plate, and then treated with 50 μl PMHNRs (50 μg/ml) for 6 h. Subsequently, individual well was washed twice with PBS buffer, and then irradiated with 808 nm diode laser (spot size: 0.5 cm) at a power density of 0.8, 2.0 and 4 W/cm^2 for 3–20 min respectively. Following irradiation, cells were cultured in DMEM medium for 2 h at 37°C. The cell viability was evaluated by the MTT assay after they were incubated with PMHNRs and irradiated with NIR laser for different time.

7

Statistical Analysis. Results from different groups were compared using one-way analysis of variance (ANOVA) by SPSS software (version 17), and p value < 0.05 was considered as statistically significant.

1. Dykman, L. & Khlebtsov, N. Gold nanoparticles in biomedical applications: recent advances and perspectives. *Chem. Soc. Rev.* **41**, 2256–2282 (2012).
2. Huang, X. H., El-Sayed, I. H., Qian, W. & El-Sayed, M. A. Cancer cell imaging and photothermal therapy in the near-infrared region by using gold nanorods. *J. Am. Chem. Soc.* **128**, 2115–2120 (2006).
3. Yuan, H., Fales, A. M. & Vo-Dinh, T. TAT peptide-functionalized gold nanostars: enhanced intracellular delivery and efficient NIR photothermal therapy using ultralow irradiance. *J. Am. Chem. Soc.* **134**, 11358–11361 (2012).
4. Hirsch, L. R. *et al.* Nanoshell-mediated near-infrared thermal therapy of tumors under magnetic resonance guidance. *Proc. Natl. Acad. Sci. U.S.A.* **100**, 13549–13554 (2003).
5. Wu, P., Gao, Y., Zhang, H. & Cai, C. Aptamer-guided silver-gold bimetallic nanostructures with highly active surface-enhanced Raman scattering for specific detection and near-infrared photothermal therapy of human breast cancer cells. *Anal. Chem.* **84**, 7692–7699 (2012).
6. Hu, K. W. *et al.* Efficient near-IR hyperthermia and intense nonlinear optical imaging contrast on the gold nanorod-in-shell nanostructures. *J. Am. Chem. Soc.* **131**, 14186–14187 (2009).
7. Cheng, L. C. *et al.* Seedless, silver-induced synthesis of star-shaped gold/silver bimetallic nanoparticles as high efficiency photothermal therapy reagent. *J. Mater. Chem.* **22**, 2244–2253 (2012).
8. Burke, A. *et al.* Long-term survival following a single treatment of kidney tumors with multiwalled carbon nanotubes and near-infrared radiation. *Proc. Natl. Acad. Sci. U.S.A.* **106**, 12897–12902 (2009).
9. Kostarelos, K., Bianco, A. & Prato, M. Promises, facts and challenges for carbon nanotubes in imaging and therapeutics. *Nat. Nanotechnol.* **4**, 627–633 (2009).
10. Liu, A. H. & Qiu, H. J. in *Graphene, carbon nanotubes, and nanostructures: techniques and applications.* (eds. J. Morris & K. Iniewski) 169–210 (CRC Press, U.S.A., Florida; 2013).
11. Huang, X. Q. *et al.* Freestanding palladium nanosheets with plasmonic and catalytic properties. *Nat. Nanotechnol.* **6**, 28–32 (2011).
12. Tang, S., Chen, M. & Zheng, N. Sub-10-nm Pd nanosheets with renal clearance for efficient near-infrared photothermal cancer therapy. *Small* **10**, 3139–3144 (2014).
13. Jain, P. K., Huang, X. H., El-Sayed, I. H. & El-Sayed, M. A. Noble metals on the nanoscale: optical and photothermal properties and some applications in imaging, sensing, biology, and medicine. *Acc. Chem. Res.* **41**, 1578–1586 (2008).
14. Zhang, L., Li, Y. C. & Yu, J. C. Chemical modification of inorganic nanostructures for targeted and controlled drug delivery in cancer treatment. *J. Mater. Chem. B* **2**, 452–470 (2014).
15. Lee, D. E. *et al.* Multifunctional nanoparticles for multimodal imaging and theragnosis. *Chem. Soc. Rev.* **41**, 2656–2672 (2012).
16. Zhang, Z. J., Wang, J. & Chen, C. H. Near-infrared light-mediated nanoplatforms for cancer thermo-chemotherapy and optical imaging. *Adv. Mater.* **25**, 3869–3880 (2013).
17. Biju, V. Chemical modifications and bioconjugate reactions of nanomaterials for sensing, imaging, drug delivery and therapy. *Chem. Soc. Rev.* **43**, 744–764 (2014).
18. Dykman, L. A. & Khlebtsov, N. G. Uptake of engineered gold nanoparticles into mammalian cells. *Chem. Rev.* **114**, 1258–1288 (2014).
19. Caruso, F. Nanoengineering of particle surfaces. *Adv. Mater.* **13**, 11–22 (2001).
20. Smith, G. P. Filamentous fusion phage - novel expression vectors that display cloned antigens on the virion surface. *Science* **228**, 1315–1317 (1985).
21. Marx, V. Calling the next generation of affinity reagents. *Nat. Methods* **10**, 829–833 (2013).
22. Lang, Q. *et al.* Specific probe selection from landscape phage display library and its application in enzyme-linked immunosorbent assay of free prostate-specific antigen. *Anal. Chem.* **86**, 2767–2774 (2014).
23. Marvin, D. A. Filamentous phage structure, infection and assembly. *Curr. Opin. Struct. Biol.* **8**, 150–158 (1998).
24. Marvin, D. A., Symmons, M. F. & Straus, S. K. Structure and assembly of filamentous bacteriophages. *Prog. Biophys. Mol. Biol.* **114**, 80–122 (2014).
25. Petrenko, V. A., Smith, G. P., Gong, X. & Quinn, T. A library of organic landscapes on filamentous phage. *Protein Eng.* **9**, 797–801 (1996).
26. Smith, G. P. & Petrenko, V. A. Phage display. *Chem. Rev.* **97**, 391–410 (1997).
27. Jayanna, P. K., Torchilin, V. P. & Petrenko, V. A. Liposomes targeted by fusion phage proteins. *Nanomedicine* **5**, 83–89 (2009).
28. Bedi, D. *et al.* Targeted delivery of siRNA into breast cancer cells via phage fusion proteins. *Mol. Pharm.* **10**, 551–559 (2013).
29. Wang, T., Petrenko, V. A. & Torchilin, V. P. Paclitaxel-loaded polymeric micelles modified with MCF-7 cell-specific phage protein: enhanced binding to target cancer cells and increased cytotoxicity. *Mol. Pharm.* **7**, 1007–1014 (2010).
30. Gandra, N., Wang, D. D., Zhu, Y. & Mao, C. B. Virus-mimetic cytoplasm-cleavable magnetic/silica nanoclusters for enhanced gene delivery to mesenchymal stem cells. *Angew. Chem., Int. Ed.* **52**, 11278–11281 (2013).
31. Li, C. C., Sun, L., Sun, Y. Q. & Teranishi, T. One-Pot controllable synthesis of Au@Ag heterogeneous nanorods with highly tunable plasmonic absorption. *Chem. Mater.* **25**, 2580–2590 (2013).
32. Knippers, R. & Hoffmann-Berling, H. A coat protein from bacteriophage Fd .I. hydrodynamic measurements and biological characterization. *J. Mol. Biol.* **21**, 281–292 (1966).
33. Spruijt, R. B., Wolfs, C. J. A. M. & Hemminga, M. A. Aggregation-related conformational change of the membrane-associated coat protein of bacteriophage M13. *Biochemistry* **28**, 9158–9165 (1989).
34. Fagbohun, O. A. *et al.* Landscape phages and their fusion proteins targeted to breast cancer cells. *Protein Eng. Des. Sel.* **25**, 271–283 (2012).
35. Schneider, G. *et al.* Distance-dependent fluorescence quenching on gold nanoparticles ensheathed with layer-by-layer assembled polyelectrolytes. *Nano Lett.* **6**, 530–536 (2006).
36. Hu, Y. F., Zandi, R., Anavitarte, A., Knobler, C. M. & Gelbart, W. M. Packaging of a polymer by a viral capsid: the interplay between polymer length and capsid size. *Biophys. J.* **94**, 1428–1436 (2008).
37. Minenkova, O. O., Ilyichev, A. A., Kishchenko, G. P. & Petrenko, V. A. Design of specific immunogens using filamentous phage as the carrier. *Gene* **128**, 85–88 (1993).
38. Qi, H., Lu, H. Q., Qiu, H. J., Petrenko, V. & Liu, A. H. Phagemid vectors for phage display: properties, characteristics and construction. *J. Mol. Biol.* **417**, 129–143 (2012).
39. Liu, A. H., Abbineni, G. & Mao, C. B. Nanocomposite films assembled from genetically engineered filamentous viruses and gold nanoparticles: nanoarchitecture- and humidity-tunable surface plasmon resonance spectra. *Adv. Mater.* **21**, 1001–1005 (2009).
40. Qi, H., Wang, F., Petrenko, V. A. & Liu, A. H. Peptide microarray with ligands at high density based on symmetrical carrier landscape phage for detection of cellulase. *Anal. Chem.* **86**, 5844–5850 (2014).
41. Yin, L. *et al.* Specific ligands for classical swine fever virus screened from landscape phage display library. *Antiviral Res.* **109**, 68–71 (2014).
42. Gray, B. P. & Brown, K. C. Combinatorial peptide libraries: mining for cell-binding peptides. *Chem. Rev.* **114**, 1020–1081 (2014).
43. Deber, C. M. *et al.* Val-Ala mutations selectively alter helix-helix packing in the transmembrane segment of phage M13 coat protein. *Proc. Natl. Acad. Sci. U.S.A.* **90**, 11648–11652 (1993).
44. Liu, Z., Qiao, J., Niu, Z. W. & Wang, Q. Natural supramolecular building blocks: from virus coat proteins to viral nanoparticles. *Chem. Soc. Rev.* **41**, 6178–6194 (2012).
45. Petrenko, V. A. & Jayanna, P. K. Phage protein-targeted cancer nanomedicines. *FEBS Lett.* **588**, 341–349 (2014).
46. Weissleder, R. A clearer vision for in vivo imaging. *Nat. Biotechnol.* **19**, 316–317 (2001).
47. Yu, C. X., Varghese, L. & Irudayaraj, J. Surface modification of cetyltrimethylammonium bromide-capped gold nanorods to make molecular probes. *Langmuir* **23**, 9114–9119 (2007).
48. Ahamed, M., AlSalhi, M. S. & Siddiqui, M. K. Silver nanoparticle applications and human health. *Clin. Chim. Acta* **411**, 1841–1848 (2010).
49. Kawata, K., Osawa, M. & Okabe, S. In vitro toxicity of silver nanoparticles at noncytotoxic doses to HepG2 human hepatoma cells. *Environ. Sci. Technol.* **43**, 6046–6051 (2009).
50. AshaRani, P. V., Low Kah Mun, G., Hande, M. P. & Valiyaveettil, S. Cytotoxicity and genotoxicity of silver nanoparticles in human cells. *ACS Nano* **3**, 279–290 (2009).
51. Silver, S., Phung, L. T. & Silver, G. Silver as biocides in burn and wound dressings and bacterial resistance to silver compounds. *J. Ind. Microbiol. Biotechnol.* **33**, 627–634 (2006).
52. Yuan, H., Khatua, S., Zijlstra, P., Yorulmaz, M. & Orrit, M. Thousand-fold enhancement of single-molecule fluorescence near a single gold nanorod. *Angew. Chem., Int. Ed.* **52**, 1217–1221 (2013).
53. Huang, J. Y., Jackson, K. S. & Murphy, C. J. Polyelectrolyte wrapping layers control rates of photothermal molecular release from gold nanorods. *Nano Lett.* **12**, 2982–2987 (2012).
54. Nel, A. E. *et al.* Understanding biophysicochemical interactions at the nano-bio interface. *Nat. Mater.* **8**, 543–557 (2009).
55. Li, Z. M. *et al.* RGD-conjugated dendrimer-modified gold nanorods for in vivo tumor targeting and photothermal therapy. *Mol. Pharm.* **7**, 94–104 (2010).
56. Boca, S. C. *et al.* Chitosan-coated triangular silver nanoparticles as a novel class of biocompatible, highly effective photothermal transducers for in vitro cancer cell therapy. *Cancer Lett.* **311**, 131–140 (2011).
57. Mahmoud, M. A. & El-Sayed, M. A. Different plasmon sensing behavior of silver and gold nanorods. *J. Phys. Chem. Lett.* **4**, 1541–1545 (2013).
58. Petrenko, V. A. & Smith, G. P. Phages from landscape libraries as substitute antibodies. *Protein Eng.* **13**, 589–592 (2000).
59. Ding, H. *et al.* Gold nanorods coated with multilayer polyelectrolyte as contrast agents for multimodal imaging. *J. Phys. Chem. C* **111**, 12552–12557 (2007).
60. Lee, S. *et al.* Biological imaging of HEK293 cells expressing PLCγ1 using surface-enhanced Raman microscopy. *Anal. Chem.* **79**, 916–922 (2007).

Acknowledgments

Author contributions

A.H.L. designed the research. F.W. and P.L. performed the experiments. C.C.L. and L.S. synthesized the Au@Ag heterogenous NRs. V.A.P. guided phage display. F.W., A.H.L. and V.A.P. analyzed data and prepared the manuscript. All authors discussed the results and revised the manuscript.

Additional information